ELSEVIER

Polymer Vol. 37 No. 10, pp. 1797–1804, 1996

0032-3861/96/$15.00 + 0.00

Molecular packing and small-penetrant diffusion in polystyrene: a molecular dynamics simulation study

Jie Han and Richard H. Boyd*
Department of Materials Science and Engineering, University of Utah, Salt Lake City, UT 84112, USA
(Received 15 May 1995; revised 23 June 1995)

Molecular dynamics (MD) simulations have been used to study bulk atactic polystyrene (aPS). A united-atom non-bonded potential is calibrated for the aromatic-ring carbons, which, along with previously determined non-bonded functions, results in a good representation of pressure–volume–temperature relations for aPS. Experimental X-ray scattering data for glassy aPS are well reproduced in simulation. Packing features in the glass are discussed in terms of various site–site radial distribution functions. Diffusion coefficients for methane as an example of a small-molecule penetrant are determined as a function of temperature in the range 380–550 K. The values from simulation when extrapolated to room temperature via an Arrhenius plot are found to be consistent with experimental values for the similar gas CO_2 at that temperature, thus implying that the glass transition in the matrix has little effect on the diffusion. The temperature behaviour of the diffusion coefficients as well as the detailed jump behaviour of the penetrant indicate that the diffusion mechanism corresponds to hopping from site to site in a solid-like medium over the temperature range studied. The lack of effect of the glass transition on diffusion is rationalized in terms of the mechanism already being hopping in a solid-like medium well above T_g. Diffusion is the slowest in aPS of any of the polymeric matrices studied so far by MD simulation. This correlates well with the fractional free volume found, which is also the lowest yet found in the polymeric matrices. Copyright © 1996 Elsevier Science Ltd.

(Keywords: polystyrene; molecular dynamics simulation; diffusion)

INTRODUCTION

Molecular dynamics (MD) simulations have become a practicable tool for studying the structure and properties of bulk amorphous polymers[1,2]. For example, they have been effective in reproducing equation-of-state or pressure–volume–temperature (*PVT*) properties and in understanding the substantial differences in the packing efficiencies of a number of hydrocarbon polymers[3–6]. These include polyethylene (PE), polyisobutylene (PIB), atactic polypropylene (aPP) and polybutadienes (PBD). Diffusion of small penetrant molecules in a polymeric host is another property that has been successfully studied[4–6]. In the present work, these studies are extended to atactic polystyrene (aPS). This polymer has probably been the most experimentally studied of all of the amorphous polymers. It is also fairly complicated in a chemical structural sense. Thus PS is an important test example for the ability of MD simulations to reproduce the salient features of bulk amorphous polymers. Static structures for aPS have been constructed via simulation using energy minimization[7,8]. MD has been used to generate structures and to study the packing features that are experimentally accessible in scattering experiments[9,10]. In this work we use MD to generate *PVT* properties, and to study the structural features of the packing and also small-molecule-penetrant diffusion. A preliminary account of aPS *V–T* curves was recently reported in the context of their use in locating glass transition temperatures in a number of polymers[11].

Our approach follows very closely our previous work[3–6], especially that on atactic polypropylene (aPP)[5]. The aromatic-ring C–H group represents for us a new structural entity, for which non-bonded potential parameters need to be calibrated. As before, the experimental isobaric *V–T* curve, isothermal *P–V* curve and cohesive energy density are used as guides in this endeavour. Then the packing features are examined in terms of site–site radial distribution functions. The diffusion of methane, as an example of a small-molecule penetrant, in the aPS host is studied. The results are then related to the diffusion behaviour of methane in other polymer hosts that we have previously studied.

SIMULATION DETAILS

Polystyrene representation

The polystyrene (*Figure 1*) simulated consisted of a single molecule of 80 monomer units. The $-CH_2-$ units were represented by 'anisotropic united-atom' (AUA) groups[12] as was done previously by us[3–6]. The aromatic-ring C(ar)–H group was also a united-atom group. As in our work on aPP, the main-chain > (C–H)– group was represented by explicit atoms. This was done because the relative number of hydrogens is small and the potentials

* To whom correspondence should be addressed

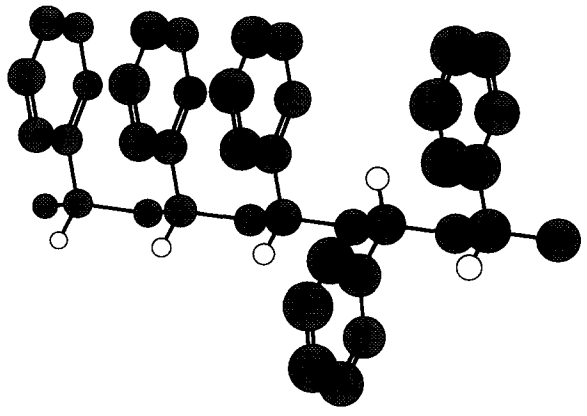

Figure 1 Representation of aPS. The aromatic > C(ar)H and the $-CH_2-$ centres are united atom. The aliphatic > (CH)– centres are explicit C, H atoms

are already available. The stereo configurations of the phenyl groups were generated at random so that the *meso* and *racemic* dyad content was near equality.

Molecular dynamics details

Procedures previously invoked by us were followed[3–6]. All of the simulations dealing with *PVT* relations were generated using constant particle number, pressure and temperature (*NPT*) dynamics. The Nosé method was used[13]. The pressure inertial parameter W was set to 10^4 atm s^2 m^{-3} and the thermal inertial parameter Q was set to 10^{-15} J s^2. The time step was taken as 0.5 fs. This relatively small value was occasioned by the inclusion of the explicit hydrogen, with its attendant small mass, at the main chain > (C–H)– group[5]. The diffusion runs were conducted under effectively *NVT* conditions at volumes established by *NPT* results. Constant V was achieved by invoking a large inertial parameter W.

The packed system was initially created by placing the chain in an all-*trans* conformation into a very large periodic box. The box was shrunk under *NPT* dynamics at high temperature until the box size stabilized. Other temperatures were obtained by cooling.

The computations were carried out on IBM RS6000/560 or /370 workstations. The CPU time was 0.08 s per time step.

For the melt temperatures studied (380, 413, 463, 500, 550 K), volume equilibration as evidenced by the volume being constant vs. time was achieved by at most 300 ps, although the equilibrations were carried out to 1 ns in the case of the three lower temperatures.

The structural characterization in terms of radial distribution functions was carried out on the glass at 300 K. This glass was prepared by cooling from intermediate-temperature isothermal equilibrations at 350 and 330 K. The glass was equilibrated for 1.5 ns before the MD sampling. The latter was carried out at 100 ps intervals over 1 ns. The glass specific volume was found to be 0.949 cm^3 g^{-1}.

The volume vs. time plots at a number of temperatures, including for both melts and glasses, were reported separately in connection with locating the volumetric glass transition temperature[11].

Potential functions

The potential function constants used are listed in *Table 1*. The bond stretching constants were selected on the basis of spectroscopic values, but all were reduced by a factor of 4 in order to increase the time step. For C–C

Table 1 Potential functions[a]

Function	Constants			
C–C bond stretch energy $= \frac{1}{2}k_R(R - R_0)^2$				
C–C	$k_R = 663$	$R_0 = 1.54$		
C(ar)–C	$k_R = 663$	$R_0 = 1.50$		
C(ar)–C(ar)	$k_R = 1100$	$R_0 = 1.39$		
C–H (in > CH–)	$k_R = 663$	$R_o = 1.09$		
Bond bending energy $= \frac{1}{2}k_\theta(\theta - \theta_0)^2$				
C–C–C	$k_\theta = 482$	$\theta_0 = 111.6°$		
C–C–H, C–C–C(ar), C(ar)–C–H, C–C–C(ar)	$k_\theta = 482$	$\theta_0 = 109.47°$		
C(ar)–C(ar)–C(ar)	$k_\theta = 602$	$\theta_0 = 120.0°$		
Torsional potential about –C–C– $\frac{1}{2}V_3[1 + \cos(3\phi)]$	$V_3 = 13.4$			
Torsional potential about –C–C(ar)– $\frac{1}{2}V_3[1 + \cos(6\phi)]$	$V_3 = 2.06$			
Torsional potential about –C(ar)–C(ar)– $\frac{1}{2}V_2[1 + \cos(2\phi)]$	$V_2 = 108$			
Non-bonded potential, Lennard-Jones 6–12[b]				
$-CH_2-$ (AUA)	$\epsilon = 0.686$	$R_{min} = 3.94$	$\sigma = 3.51$	$d = 0.42$
> C(ar)H (AUA)[c]	$\epsilon = 0.536$	$R_{min} = 4.22$	$\sigma = 3.76$	$d = 0.0$
> C < (in > CH–) (explicit atom)[d]	$\epsilon = 0.397$	$R_{min} = 3.872$	$\sigma = 3.45$	
H (in > CH–) (explicit atom)[d]	$\epsilon = 0.041$	$R_{min} = 3.37$	$\sigma = 3.00$	
CH_4 (UA)	$\epsilon = 1.18$	$R_{min} = 4.27$	$\sigma = 3.80$	$(d = 0)$

[a] Energies in kJ mol^{-1}, distances in Å, angles in radians (shown above in degrees). Unless otherwise noted, the potentials are from refs 3 and 5

[b] For the $-CH_2-$ group, the potential is of the AUA (anisotropic united-atom) type; the interaction centre is offset from the C atom by the distance d along the bisector of the C–C–C angle in the direction of the hydrogens; from ref. 3. For the phenyl ring, C(ar)–H was taken to be AUA but $d = 0.0$ was found to give good results and thus is actually UA (united atom); the methane potential is united atom, UA; ϵ is the well depth; R_{min} the distance at the minimum; σ is the distance at the energy zero

[c] Parametrized in this work

[d] From ref. 5

and C–H the values were the same as previously employed[3,5]. For the aromatic-ring bonds, C(ar)–C(ar), a value from the MOLBD3 force field[14] was used (these parameters are available in the POLYMER module in the SYBYL simulation software of the Trios Co., St Louis, MO) and attenuated by 4×. For the C–C(ar) bond attaching the ring to the chain, the aliphatic C–C force constant was used, but the relaxed length was shortened appropriately. The C–C–C angle bend function is the same as previously used[3,5]. The same force constant was invoked for all of the bends involving aliphatic carbon as the centre atom. However, the exact tetrahedral value for the relaxed angle was used rather than the larger value that obtains in a C–C–C sequence. The C(ar)–C(ar)–C(ar) bend force constant was taken from the MOLBD3 force field. The torsional potential about –C–C– is the same as previously used[3,5]. The aromatic ring planarity is accomplished via a two-fold rotational potential. The barrier is from the MOLBD3 force field. The intrinsic –C–C(ar)– torsional barrier is considered to be very low. It is essentially zero in toluene[15]. However, when attached to the aliphatic carbon main chain, non-bonded interactions cause a substantial barrier[16]. The united-atom formulation decrease these and a modest barrier is invoked explicitly.

The $-CH_2-$ AUA non-bonded potential has been used previously[3,5]. The C and H explicit-atom potentials in the > (C–H)– group are the same as used in aPP[5]. The united-atom C(ar)–H group in the aromatic rings was calibrated here. It was assumed to be of the AUA type. The ϵ and σ parameters were adjusted by calculating the volume and cohesive energy density at 413 K for several assumed fixed values of the AUA offset d. It was found that a better representation of the V–T curve as well as the cohesive energy density could be effected for small values of d than for larger ones (in the range of several tenths of an ångström). Thus the value $d = 0.0$ was selected and the ϵ and σ parameters adjusted for this d value.

Diffusion

Methane was chosen as the penetrant to conform with our earlier studies on diffusion in a number of other polymers[4–6]. A single penetrant was used at higher temperatures (463, 500, 550 K). To improve the diffusion statistics, four penetrants were used at 380 and 413 K. After *NPT* volume equilibration, the penetrants were introduced in the periodic box of dimensions determined by the volume equilibration. At the low penetrant concentration involved (one or four particles in 720), the density error involved is minor. The penetrant-containing systems were re-equilibrated for several hundred picoseconds before collecting diffusion data. The diffusion coefficient was determined from one-sixth of the slope of $\langle R_p^2 \rangle$ vs. time, where R_p is the distance moved by the penetrant from the $t = 0$ origin. The averaging implied in $\langle R_p^2 \rangle$ is accomplished by the usual practice of starting new origins (in this case every 1 ps) along the trajectory[17] and by averaging the multiple penetrant trajectories in the appropriate cases. The trajectories were continued until the diffusional slope was clearly separable from both the early-time cage effect and the later-time noise associated with disappearance of multiple trajectories near the end of the run.

RESULTS AND DISCUSSION

PVT results

The properties used in calibrating the aromatic-ring non-bonded C(ar)H united-atom potential are considered first. The volume vs. temperature for aPS melts is shown in *Figure 2*. Also shown are experimental results from the compilation by Zoller[18]. The agreement between them is good. The solubility parameter δ was calculated from $\delta = (\Delta E/V)^{1/2}$, where ΔE is the cohesive energy and V is the volume. The cohesive energy was taken to be the intermolecular non-bonded energy[3]. The solubility parameter was found to be 17.8 $Pa^{1/2}$ at 300 K and 16.3 $Pa^{1/2}$ at 413 K. Experimental values of δ from the compilation by Grulke[19] are 18.5 ± 1 at 300 K and 15.6 $Pa^{1/2}$ at 413 K. Considering the scatter in reported values, the agreement is satisfactory. This assessment is to be tempered by the realization that the experimental values tend to be indirectly determined, such as via swelling experiments. Nevertheless, reproducing the solubility parameter behaviour is encouraging with respect to proper calibration of the non-bonded potential.

A pressure vs. volume isotherm at 500 K is shown in *Figure 3*. Experimental results are also shown[18]. It is observed that the agreement is good.

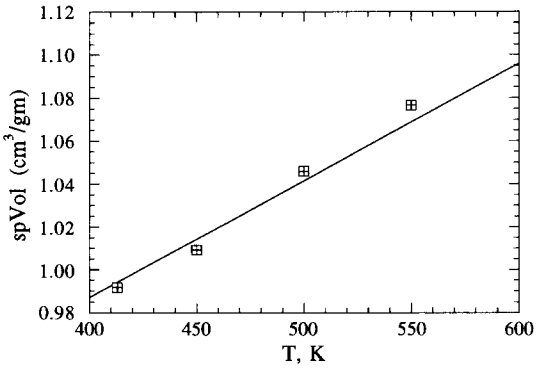

Figure 2 Specific volume vs. temperature at zero pressure. The points are from MD simulation. The full line is experimental, from ref. 18

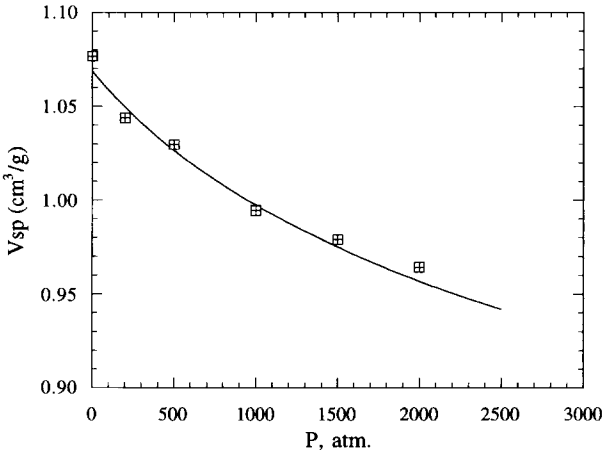

Figure 3 Specific volume vs. pressure at 500 K. The points are from MD simulation. The full curve is experimental, from ref. 18

Structural characterization

In this section, some of the structural features concerning the intermolecular packing and the internal structure are addressed. This is done chiefly through various site–site pair correlation functions. There are experimental data concerning the overall structure from wide-angle X-ray scattering measurements[20]. This is taken up first.

Comparison with X-ray scattering experiments. Scattering experiments measure intensity as a function of scattering vector q. Simulations can accumulate, via sampling the atom positions, radial distribution functions (RDFs) that express the probability of finding another centre of a specified type at a distance R from a given centre type. After subtracting the independent scattering from the atom centres to form a reduced intensity function, the experiments are related to the simulations in a straightforward manner via Fourier transforms of the radial distribution functions[9,20–22]. Experimentally, the q-dependent reduced scattering intensity $I(q)$ is found from the corrected scattered intensity $I_{corr}(q)$ and atomic scattering factors $f_i(q)$ as:

$$I(q) = kI_{corr}(q) - \sum_i f_i^2(q) \quad (1)$$

where k is a normalization. In terms of atomic positions, $I(q)$ is given by[9,22]:

$$I(q) = \bar{\rho}\int_0^\infty d_r 4\pi r^2 [x_C^2 f_C(q)^2 h_{CC}(r) + 2x_C x_H f_C(q) f_H(q) h_{CH}(r) + x_H^2 f_H(q)^2 h_{HH}(r)] \frac{sin(qr)}{qr} \quad (2)$$

where the $h(r)$ functions are net radial distribution functions, $h(r) = g(r) - 1$, where $g(r)$ is a radial distribution function. The functions $f(q)$ are atomic scattering factors and $\bar{\rho}$ the average density.

Pair radial distribution functions $g_{CC}(r)$, $g_{CH}(r)$ and $g_{HH}(r)$ were determined in MD runs on the glass at 300 K. In accomplishing this for the g_{CH} and g_{HH} functions, the hydrogen positions at $-CH_2-$ and C(ar)–H were determined by geometric construction. The g functions were used in equation (2), along with atomic scattering factors $f_C(q)$ and $f_H(q)$ taken from Alexander[21], to calculate the reduced intensity $I(q)$. The calculated and experimental q-weighted reduced intensity functions $qI(q)$ are compared in *Figure 4*. It may be seen that the agreement is good. Mondello *et al.*[9] also obtained good agreement between their united-atom MD simulation structure of PS and the X-ray scattering data.

Structural features of the packing. The complete radial distribution function, which includes distances between all carbon centres as well as the explicit hydrogen at > (C–H)–, but no constructed hydrogens as were used in computation of the X-ray scattering intensity above, is shown in *Figure 5*. Also shown there is the distribution function resolved into *inter* and *intra* components. The classification of the distances as *inter* or *intra* in a single chain system has been described previously[3]. The $g(r)$ based on main-chain C···C pairs, including both $-CH_2-$ and > (C–H)– types, are shown in *Figure 6*. Functions for the phenyl-ring C(ar) atoms are displayed in *Figure 7*.

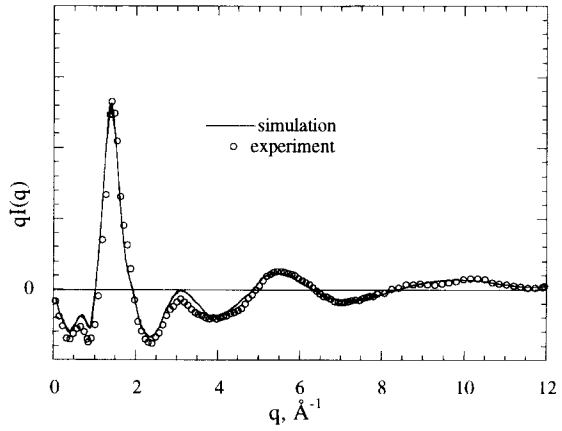

Figure 4 The X-ray scattering intensity, weighed by q, vs. q, from MD simulation compared with experiment. The data are from ref. 20

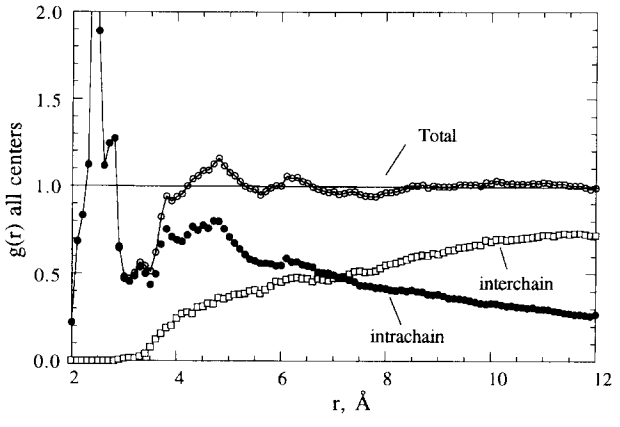

Figure 5 The overall radial distribution function $g(r)$ vs. r. It is also resolved into intermolecular and intramolecular components

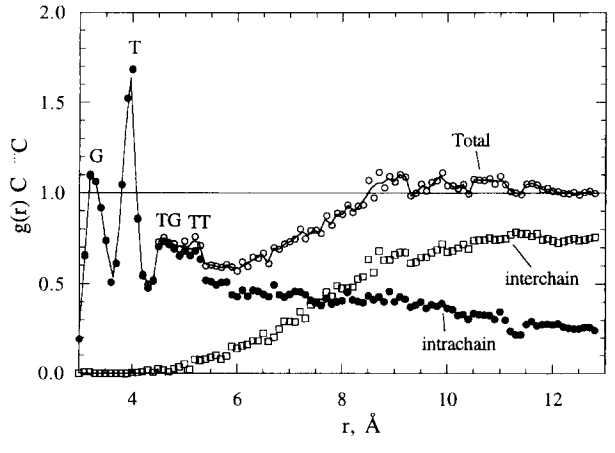

Figure 6 Site–site pair distribution function for aliphatic carbons (and therefore main chain) to aliphatic carbons. It is also resolved into intermolecular and intramolecular components. The intermolecular *trans* conformation end atom separation is labelled (*T*) as is the corresponding *gauche* distance (*G*). The end atom distances for *TT* and *TG* sequences are also labelled.

In *Figure 6*, peaks appearing at distances corresponding to the terminal atoms in *trans* (*T*) and *gauche* (*G*) conformations are labelled in the C···C $g(r)$. The peaks indicate a higher *trans* population than *gauche*. From peak height alone the *T*/*G* ratio is approximately 60/40. Since the *gauche* peak should be expected to be somewhat broader than the *trans*, owing to torsional oscillations being ineffective in changing the distance in the *trans*, this ratio is probably an overestimate. From direct sampling of the torsional angle values during simulation, the *T*/*G* ratio was found to be 0.55/0.45. Also labelled in *Figure 6* are distances corresponding to *TT* and *TG* sequences. The peaks are consistent with comparable *trans* and *gauche* populations. The static simulations by Khare *et al.*[7] and Rapold *et al.*[8] reported *trans* and *gauche* populations similar to the ones found here.

The phenyl-ring aromatic carbon $g(r)$ functions in *Figure 7* show two peaks in both the *intra* and *inter* functions. The shorter distance, 4.5–5.0 Å, corresponds to the closest individual contacts between aromatic carbons on different but nearby rings. The feature at ~ 6 Å is presumably due to the slightly more distant remaining atoms in the ring. The fact that the *intra* function shows these features prominently implies that conformations that bring adjacent rings near each other are common. This corresponds to conformations generating four bond 'ω' interactions in the language of rotational isomeric state models[23]. Thus apparently *TT* sequences in *meso* dyads and *TG* sequences in *racemic* ones are common. As already noted above the populations found are consistent with this. It has long been appreciated that the phenyl···phenyl ω interactions are much less sterically severe in aPS than the methyl···methyl interferences in its counterpart, aPP[16,24]. In fact they appear to be attractive, rather than repulsive, in molecular mechanics calculations that do not include the solvating effect of a bulk medium[24–26]. The principal reasons for these facts are that the flat surfaces of the phenyl rings provide opportunity for coordination of the rings and also that the van der Waals 'half-thickness' of the π cloud of the phenyl ring is substantially less than the van der Waals radius of a methyl group.

Turning to the intermolecular packing, it may be seen in *Figure 5* that the overall intermolecular $g(r)$ is rather featureless. The $g(r)$ based only on main-chain carbons, in *Figure 6*, is somewhat more revealing in that it appears to have a broad feature in the ~ 11 Å region. At this point a comparison of the interchain features with the behaviour found in other systems is in order. In *Figure 8* previous[5] interchain $g(r)$ functions based on main-chain C···C pairs for PE, aPP and PIB are compared with aPS. In the simplest case, PE, the interchain function has a prominent maximum at slightly more than 5 Å. This has been attributed to the neighbour spacing in a rough model where the chains pack locally as parallel cylinders[3,27,28]. The second-neighbour spacing is even discernible at ~ 10 Å. For the other chains the interchain spacings are less prominent but nevertheless appear to be discernible as marked in the figure. Since all of the chains have two main-chain carbon atoms per repeat, the interchain spacings are expected to increase with the carbon atoms in the repeat unit as PE → aPP → PIB → aPS, and this is observed.

The contacts between chains are of interest. These can be expressed in an intermolecular distribution function based on the distance between pendent centres, $-CH_3$ (for aPP, PIB) or C(ar) (for aPS) and any other type of centre. These functions are compared in *Figure 9*. Features corresponding to the close contact between a

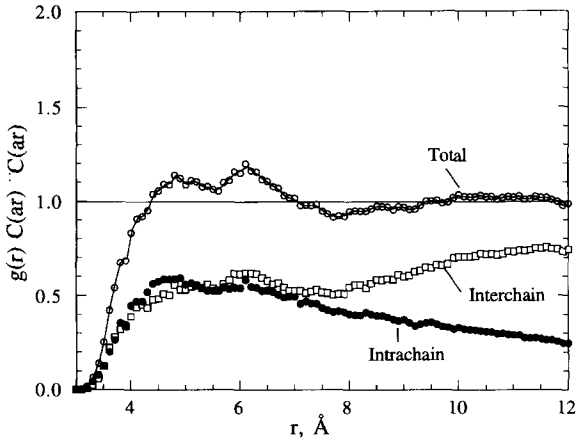

Figure 7 Site–site pair distribution function for aomatic carbons (and therefore phenyl ring) to aromatic carbons. It is also resolved into intermolecular and intramolecular components

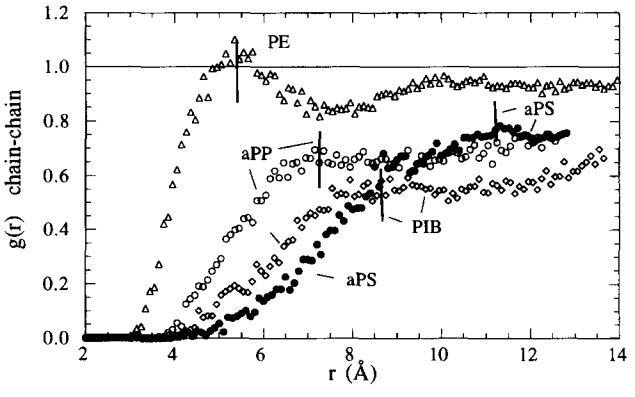

Figure 8 Comparison of intermolecular site–site main-chain carbon atom C···C distribution functions for PE, aPP, PIB and aPS. The data for the first three are from ref. 5. Approximate chain–chain spacings are marked by vertical bars

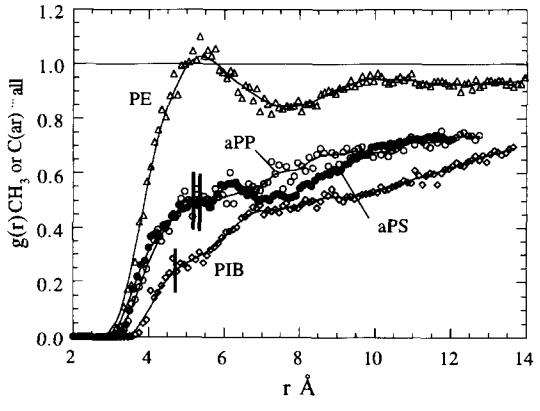

Figure 9 Site–site pair function for side-group atoms to any other atom, main chain or side group, compared for aPP, PIB and aPS. For aPP and PIB the side groups are $-CH_3$ groups, while for aPS they are phenyl-ring carbons. PE is also shown for comparison, same data as in *Figure 8*

Table 2 Fractional free volumes in polymeric hosts at 400 K

Polymer	*FFV*	Ref.
PE	0.420	5
aPP	0.415	5
PIB	0.355	5
cis-PBD	0.463	6
aPS	0.317	this work

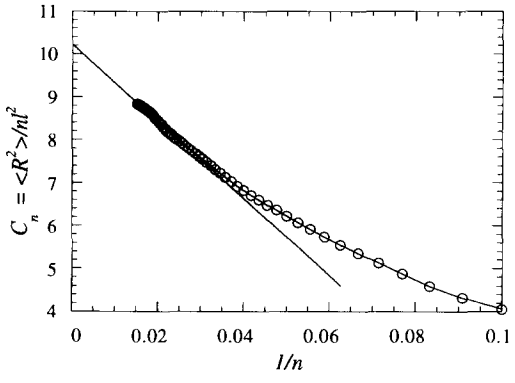

Figure 10 Characteristic ratio for aPS plotted against $1/n$, where n is the number of bonds in a connected sequence. The line indicates the extrapolation to the high-molecular-weight limit. The simulation data are at 400 K

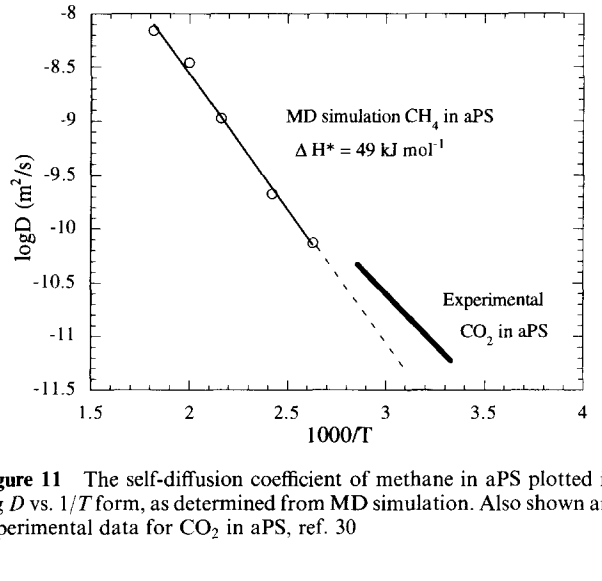

Figure 11 The self-diffusion coefficient of methane in aPS plotted in log D vs. $1/T$ form, as determined from MD simulation. Also shown are experimental data for CO_2 in aPS, ref. 30

pendent centre and another chain are marked as vertical lines. It may be seen that PIB has the closest contact distance. The distances in aPP and aPS are nearly the same. The fact that the PIB curve falls below the aPP curve at these distances is attributed to the greater chain thickness in the latter depleting the interchain contacts. This latter effect is not observed for aPS and is presumed to be due to the greater number of pendent group centres and their close proximity due to intermolecular interleaving.

Free-volume analysis. The free volume was defined as that volume not enclosed in van der Waals spheres about the constituent centres. The sphere diameters were taken as the σ values listed in *Table 1*. The free volume was determined by sampling the system at intervals when a large number of points were inserted at random in the simulation box. The fractional free volume is the fraction of such points that lie in unoccupied space. The fractional free volume was found to be 0.335 at 413 K and 0.387 at 450 K. The value at 400 K by linear extrapolation is 0.317. Values at 400 K found for aPS and for other polymers by the same procedure in previous simulations[3–6] are shown in *Table 2*. aPS has the smallest fractional free volume of any of the polymers studied by us so far.

Characteristic ratio. Another molecular feature of interest is the characteristic ratio. This is defined[23] as $C_n = \langle R^2 \rangle / nl^2$ where $\langle R^2 \rangle$ is the mean-square end-to-end distance, n is the number of main-chain bonds and l is their length. Experimental values in the high-molecular-weight limit are available. In simulation, inter-centre distances that are greater than half the box size are not reliable due to artifacts introduced by the periodic boundary conditions. However intramolecular main-chain atom separations R_{ij}^2 can be accumulated as a function of separation $n = | i - j |$ and extrapolated against n. The valid range of n is high enough that a meaningful value of $C_{n \to \infty}$ can be obtained. The result is shown in *Figure 10* where a value of C_∞ of ~ 10.2 is indicated. The reliability with respect to the extrapolation itself is probably of the order ± 0.3. Experimental values of 10.0 and 9.5 have been tabulated[23,29].

Diffusion

Simulation results. The self-diffusion coefficients of methane in aPS at five temperatures (380, 413, 463, 500 and 550 K) are shown in a log D vs. $1/T$ plot in *Figure 11*. The plot is linear within the reliability of the data with an attendant activation energy of 49 kJ mol^{-1}. Also shown in *Figure 11* are experimental data for CO_2 as penetrant in aPS[30] in the vicinity of room temperature. The latter gas diffuses 1.5–2 times faster than CH_4 in several polymeric hosts and with an activation energy 4–8 kJ mol^{-1} smaller[30]. The dashed line extrapolation in *Figure 11* gives a room-temperature diffusion coefficient for CH_4 that is three times smaller than that for CO_2. Thus it appears that Arrhenius extrapolation of the MD results is consistent with experimental results in the glass at room temperature. The inference that the glass transition does not have a direct effect on the diffusion is an important consideration, and has been the subject of earlier investigation and comment[30]. We return to this question after discussing the diffusion mechanism in more detail below.

Diffusion mechanism. It is important to put the penetrant diffusion behaviour in aPS into context with that found in other systems. A summary of previous simulation and experimental results[4–6] is given in *Figure 12*. Both in previous simulations and experimentally there is a tendency for the diffusion coefficients of small-molecule penetrants like methane to have an activation energy at lower temperatures in the range found for aPS. However, there is also a tendency, if the temperature range is wide enough, for the Arrhenius plot to be curved and for the activation energy to decrease at higher temperature. PE, aPP and *cis*-PBD are examples

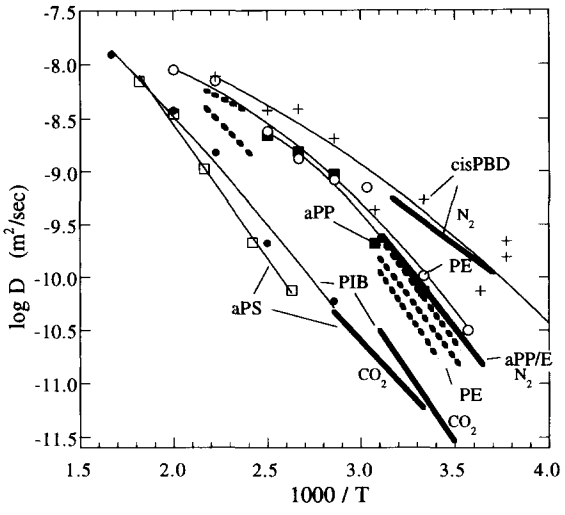

Figure 12 Summary of small-penetrant diffusion coefficient behaviour for *cis*-PBD, aPP, PE, PIB and aPS. The points are from MD simulation and methane is the diffusant in all cases. The thin curves smooth the MD data. The heavy lines are experimental data: the diffusants are marked, but are either N_2 or CO_2. The data marked aPP/E are for ethylene/propylene copolymers. The heavy dotted lines are experimental data from a variety of sources for methane in PE. The latter data have been corrected for crystallinity, see ref. 4. See refs 4–6 for sources of the data

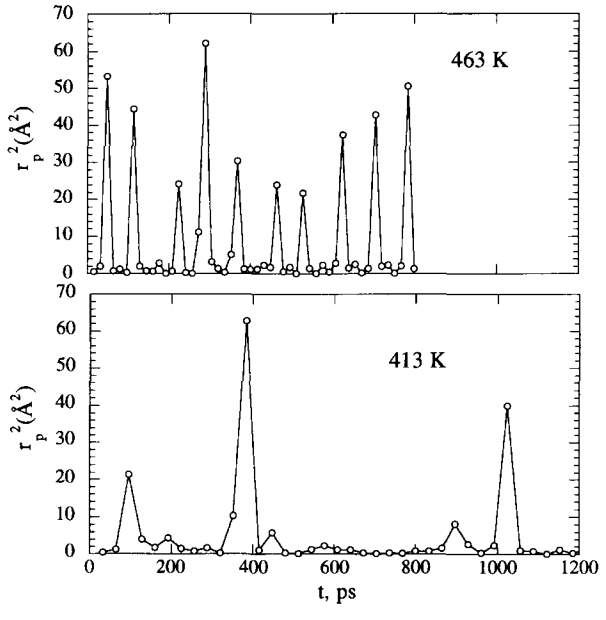

Figure 13 Temporal jump map for a single penetrant in aPS. The squared displacement r_p^2 is computed between successive positional averages. At 413 K the averaging interval is 32 ps and at 450 K it is 16 ps

where this more complex behaviour occurs. Compared to these three polymers, penetrant diffusion in PIB is considerably slower at the same temperature. Only slight curvature in the plot is observed. In aPS diffusion is slower still, which is consistent with Arrhenius behaviour over the entire range studied.

In our previous work we have ascribed the curvature of the Arrhenius plots and drop in activation energy to a gradual change in the mechanism of diffusion as temperature increases. At low temperature the diffusant tends to be trapped for long periods in a cage of solid-like

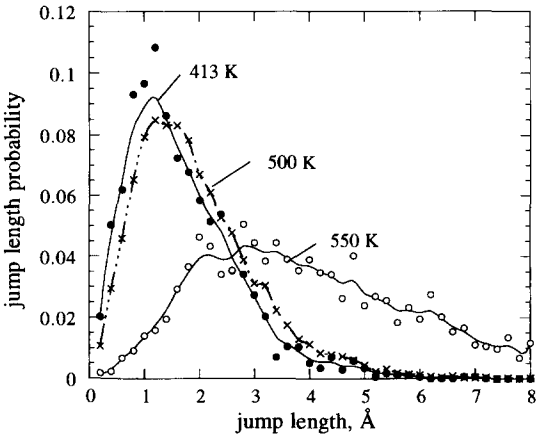

Figure 14 The distribution of jump lengths for a penetrant in aPS at various temperatures. The averaging interval is 8 ps at 500 K and 4 ps at 550 K. The curves serve as a guide to the eye and were created by a smoothing spline

surrounding polymer. Occasional large jumps to new sites take place. At higher temperature the jumps become more frequent until they are not well resolved with time and the movement is a more liquid-like scattering process. We have used two diagnostic measures of this behaviour[4]. One is to plot the jumps vs. time. The other is to determine a jump-length probability distribution. Both require filtering out the 'noise' associated with cage motions. This is done by computing the average position of the diffusant over a time interval. If the interval is chosen long enough, the noise is filtered. If it is short enough, consecutive intervals define a trajectory that captures most of the motion connected with diffusive movement.

A time-resolved jump map is shown in *Figure 13* for two temperatures. At 413 K it is clear that the low-temperature solid-like hopping process is operative. At 463 K even though the jumps are much more frequent they are still well resolved, indicating that the hopping region is still operative. The jump-length distribution is shown in *Figure 14*. At 413 K and even at 500 K the distribution is fairly sharply peaked. By 550 K the distribution has broadened and the average jump size has increased considerably. This indicates a transition to the more liquid-like region of diffusive motion. In *Figure 15* jump-length distributions for PE, aPP and PIB at 400 K are compared to the 413 K aPS distribution of *Figure 14*. At similar temperatures, aPS and PIB, the two slow diffusion media, show comparable behaviour and the faster non-Arrhenius diffusion media PE and aPP have broader distributions with much longer average jump lengths.

Effect of the glass transition. The influence of the host glass transition on the diffusion rates of small penetrants has been the subject of previous interest[30]. Early work[31] on gases in poly(vinyl acetate) (PVAc) indicated that diffusion in the glass was *faster* rather than slower with *smaller* activation energy than given by Arrhenius extrapolation from above T_g. However, other work[32] on a variety of gases in poly(ethyl methacrylate) showed no effect at all of going through T_g on the Arrhenius temperature behaviour. The MD behaviour found here appears to be consistent with this latter behaviour. The

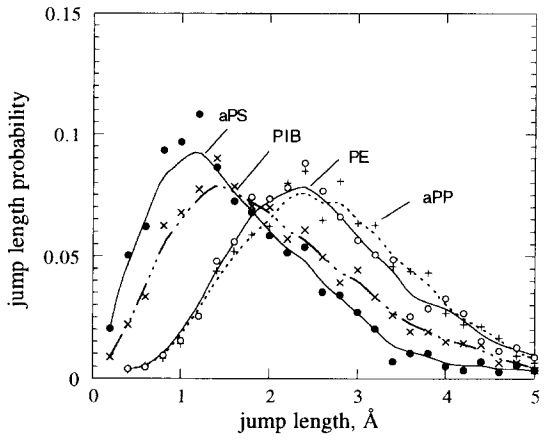

Figure 15 The distribution of jump lengths compared for PE, aPP, PIB and aPS. For the first three the temperature is 400 K and for aPS it is 413 K. The curves serve as a guide to the eye and were created by a smoothing spline

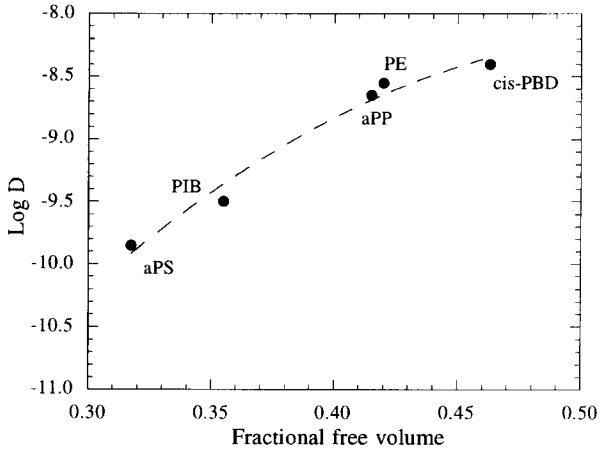

Figure 16 Free volume and diffusion. The logarithm of the diffusion coefficient at 400 K for PE, aPP, PIB, *cis*-PBD and aPS plotted against fractional free volume at the same temperature

lack of effect of T_g on the temperature dependence of small-penetrant diffusion can be rationalized in terms of the mechanism discussed above.

The transition in diffusion mechanism to the solid-like hopping mode takes place *well above* the glass transition in the cases studied. This apparently is a consequence of the very short-time nature of diffusive jumps for small diffusants. The reduction in longer-range segmental mobility that the host undergoes in the glass transition region appears to have little effect on diffusants already undergoing cage motion with occasional diffusional jumps.

A practical consequence of the above is that MD simulations on small penetrants carried out at temperatures where the mechanism is already in the hopping regime can probably be extrapolated to lower temperature even if the glass transition intervenes.

Free volume and diffusion. Free volume is a frequently invoked concept in rationalizing diffusion phenomena. We have found the free volume in the polymeric host matrix to be remarkably successful in ordering the diffusion rates for the same penetrant among various polymers[5]. *Figure 16* shows log D for methane plotted against the fractional free volume at 400 K for the five polymer hosts that we have studied so far[4–6]. A close correlation between diffusion coefficient and free volume is observed.

ACKNOWLEDGEMENTS

The authors are grateful to The Exxon Chemical Company (diffusion work) and to the Polymers Program, Division of Materials Research, National Science Foundation (*PVT* work) for financial support of this work. They are also indebted to the Utah Supercomputing Institute for use of their facilities. Conversations with Dr G. Ver Strate concerning diffusion have been very helpful.

REFERENCES

1 'Computer Simulation of Polymers' (Ed. R. J. Roe), Prentice Hall, New York, 1991
2 'Atomistic Modeling of Physical Properties of Polymers' (Eds. L. Monnerie and U. Suter), Springer, New York, 1994
3 Pant, P. V. K., Han, J., Smith, G. D. and Boyd, R. H. *J. Chem. Phys.* 1993, **99**, 597
4 Pant, P. V. K. and Boyd, R. H. *Macromolecules* 1993, **26**, 679
5 Han, J. and Boyd, R. H. *Macromolecules* 1994, **27**, 5365
6 Gee, R. H. and Boyd, R. H. *Polymer* 1995, **36**, 1435
7 Khare, R., Paulitis, M. E. and Lustig, S. R. *Macromolecules* 1993, **26**, 7203
8 Rapold, R. F., Suter, U. W. and Theodorou, D. N. *Macromol. Theory Simul.* 1994, **3**, 19
9 Mondello, M., Yang, H. J., Furuya, H. and Roe, R. J. *Macromolecules* 1994, **27**, 3566
10 Furuya, H., Mondello, M., Yang, H. J., Roe, R. J., Erwin, R. W., Han, C. C. and Smith, S. D. *Macromolecules* 1994, **27**, 5674
11 Han, J., Gee, R. H. and Boyd, R. H. *Macromolecules* 1994, **27**, 7781
12 Toxvaerd, S. *J. Chem. Phys.* 1990, **93**, 4290
13 Nosé, S. *J. Chem. Phys.* 1984, **81**, 511
14 Boyd, R. H., Breitling, S. M. and Mansfield, M. L. *AIChE J.* 1973, **19**, 1016
15 Pitzer, K. S. and Scott, D. W. *J. Am. Chem. Soc.* 1943, **65**, 803
16 Yoon, D. Y., Sundararanjan, P. R. and Flory, P. J. *Macromolecules* 1975, **8**, 776
17 Jolly, D. L. and Bearman, R. J. *Mol. Phys.* 1980, **41**, 137
18 Zoller, P. 'PVT relations and equations of state of polymers' in 'Polymer Handbook', 3rd Edn. (Eds. J. Brandrup and E. H. Immergut), Wiley-Interscience, New York, 1989
19 Grulke, E. A. 'Solubility parameter values' in 'Polymer Handbook', 3rd Edn. (Eds. J. Brandrup and E. H. Immergut), Wiley-Interscience, New York, 1989
20 Mitchell, G. R. and Windle, A. H. *Polymer* 1984, **25**, 906
21 Alexander, L. E. 'X-ray Diffraction Methods in Polymer Science', Wiley, New York, 1969
22 Pings, C. J. and Waser, J. *J. Chem. Phys.* 1968, **48**, 3016
23 Flory, P. J. 'Statistical Mechanics of Chain Molecules' Interscience, New York, 1969
24 Stegen, G. E. and Boyd, R. H. *Polym. Prepr.* 1978, **19(1)**, 595
25 Gorin, S. and Monnerie, L. *J. Chim. Phys.* 1970, **67**, 869
26 Farmer, B. L. and Lando, J. B. *J. Macromol. Sci. (B) Phys.* 1974, **10**, 381
27 Rigby, D. and Roe, R. J. *J. Chem. Phys.* 1988, **89**, 5280
28 Pant, P. V. K. and Boyd, R. H. *Macromolecules* 1991, **24**, 6235
29 Fetters, L. J., Lohse, D. J., Richter, D., Witten, T. A. and Zirkel, A. *Macromolecules* 1994, **27**, 4639
30 Stannett, V. in 'Diffusion in Polymers' (Eds. J. Crank and G. S. Park), Academic Press, New York, 1968, Ch. 2
31 Mears, P. *J. Am. Chem. Soc.* 1954, **76**, 3415
32 Stannett, V. and Williams, J. L. *J. Polym. Sci. (C)* 1966, **10**, 45